ac Stark Shift and Dephasing of a Superconducting Qubit Strongly Coupled to a Cavity Field

D. I. Schuster, A. Wallraff, A. Blais, L. Frunzio, R.-S. Huang,* J. Majer, S. M. Girvin, and R. J. Schoelkopf Departments of Applied Physics and Physics, Yale University, New Haven, Connecticut 06520, USA (Received 16 August 2004; published 30 March 2005)

We have performed spectroscopy of a superconducting charge qubit coupled nonresonantly to a single mode of an on-chip resonator. The strong coupling induces a large ac Stark shift in the energy levels of both the qubit and the resonator. The dispersive shift of the resonator frequency is used to nondestructively determine the qubit state. Photon shot noise in the measurement field induces qubit level fluctuations leading to dephasing which is characteristic for the measurement backaction. A crossover in line shape with measurement power is observed and theoretically explained. For weak measurement a long intrinsic dephasing time of $T_2 > 200$ ns of the qubit is found.

DOI: 10.1103/PhysRevLett.94.123602

The investigation of strong coupling between a single quantum two-level system and a single photon, as first realized in atomic cavity quantum electrodynamics (CQED) [1], is not only at the forefront of research in quantum optics and atomic physics [2] but also has great prospects in the realm of quantum information processing [3] where realizing entanglement between qubits and photons is essential for quantum communication. Recently, it has been proposed [4] and demonstrated for the first time in a solid state system that strong coupling CQED [5,6] can be realized in superconducting quantum circuits [7]. Following these results, strong coupling has also been achieved in a second solid state system, namely, semiconducting quantum dots embedded in microcavities [8,9]. In this Letter we demonstrate the use of *nonresonant* (dispersive) strong coupling between a Cooper pair box (CPB) [10] and a coherent microwave field in a high quality transmission line resonator to measure the quantum mechanical state of the Cooper pair box in a quantum nondemolition (OND) scheme [4,11,12]. The interaction between the Cooper pair box and the measurement field containing n photons on average gives rise to a large ac Stark shift of the qubit energy levels, analogous to the one observed in CQED [13], demonstrated here for the first time in superconducting qubits. As a consequence of the strong coupling, quantum fluctuations in n induce a broadening of the transition linewidth, which represents the backaction of the measurement on the qubit.

In our circuit QED architecture [4] [see Fig. 1(a)] a split Cooper pair box [10], modeled by the two-level Hamiltonian $H_a=-1/2(E_{\rm el}\sigma_x+E_{\rm J}\sigma_z)$ [14], is coupled capacitively to the electromagnetic field of a full wave $(l=\lambda)$ transmission line resonator, described by a harmonic oscillator Hamiltonian $H_{\rm r}=\hbar\omega_{\rm r}(a^{\dagger}a+1/2)$. In the Cooper pair box, the energy difference $E_a=\hbar\omega_a=(E_{\rm el}^2+E_{\rm J}^2)^{1/2}$ between the ground state $|\downarrow\rangle$ and the first excited state $|\uparrow\rangle$ [see Fig. 1(b)], is determined by its electrostatic energy $E_{\rm el}=4E_{\rm C}(1-n_{\rm g})$ and its Josephson coupling energy $E_{\rm J}=E_{\rm J,max}\cos(\pi\Phi_{\rm b})$. Here, $E_{\rm C}=e^2/2C_{\Sigma}\approx 5$ GHz is the charging energy given by the total

PACS numbers: 42.50.Pq, 32.60.+i, 42.50.Lc, 85.35.Gv

box capacitance C_{Σ} , $n_{\rm g}=C_{\rm g}^{\star}V_{\rm g}/e$ is the gate charge controlled by the gate voltage $V_{\rm g}$ applied through a gate with effective capacitance $C_{\rm g}^{\star}$, and $E_{\rm J,max}\approx 8$ GHz is the maximum Josephson coupling energy of the two junctions which is modulated by applying a flux bias $\Phi_{\rm b}=\Phi/\Phi_0$ to the loop of the split box [see Fig. 1(a)]. $\Phi_0=2e/h$ is the magnetic flux quantum. Near its resonance frequency $\omega_r=1/\sqrt{LC}\approx 2\pi$ 6 GHz, the resonator is accurately modeled as a harmonic oscillator with lumped inductance L and capacitance C.

In the presence of strong mutual coupling between the qubit and the resonator [5], their *dressed* excitation ener-

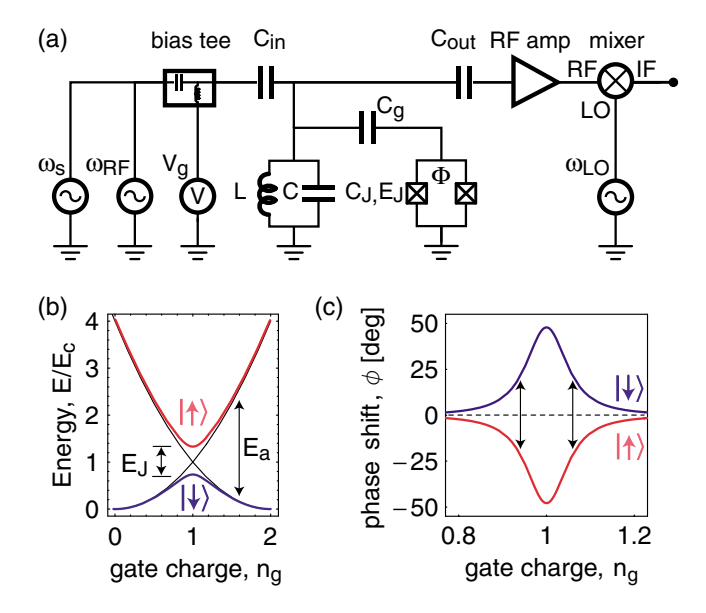


FIG. 1 (color online). (a) Simplified circuit diagram of measurement setup. The phase ϕ and amplitude T of a microwave at $\omega_{\rm rf}$ transmitted through the resonator, amplified, and mixed down to an intermediate frequency $\omega_{\rm IF} = \omega_{\rm rf} - \omega_{\rm LO}$ using a local oscillator at $\omega_{\rm LO}$ is measured. An additional spectroscopy microwave at $\omega_{\rm s}$ is applied to the input port of the resonator. (b) Ground $|\downarrow\rangle$ and excited $|\uparrow\rangle$ state energy levels of CPB vs gate charge n_g . (c) Calculated phase shift ϕ in ground and excited states vs n_g for $\Delta_{\rm a,r}/2\pi=100$ MHz.

gies $\tilde{\omega}_a$ and $\tilde{\omega}_r$, are modified from their bare values ω_a and ω_r . For large detuning $\Delta_{a,r} = \omega_a - \omega_r$ the dressed energy levels are determined by the Hamiltonian [4]

$$H \approx \hbar \left(\omega_{\rm r} + \frac{g^2}{\Delta_{\rm a,r}}\sigma_z\right) a^{\dagger} a + \frac{1}{2} \hbar \left(\omega_{\rm a} + \frac{g^2}{\Delta_{\rm a,r}}\right) \sigma_z,$$
 (1)

where $g/2\pi \approx 5.8$ MHz is the coupling strength between a single photon and the qubit [5]. In this nonresonant case, the dressed resonator frequency $\tilde{\omega}_{\rm r} = \omega_{\rm r} \pm g^2/\Delta_{\rm a,r}$ depends on the qubit state $\sigma_z = \pm 1$ and the detuning $\Delta_{\rm a,r}$. The qubit state can thus be inferred from the phase shift ϕ that a probe microwave transmitted through the resonator at frequency $\omega_{\rm rf}$ experiences because of the interaction with the qubit [4,5]. In Fig. 1(c), the expected phase shift $\phi = \pm \tan^{-1}(2g^2/\kappa\Delta_{\rm a,r})$, where $\kappa = \omega_{\rm r}/Q$ is the decay rate of photons from the resonator with quality factor $Q \approx 10^4$, is plotted versus gate charge $n_{\rm g}$. ϕ is maximum at $n_{\rm g} = 1$ where the detuning $\Delta_{\rm a,r}$ is smallest and falls off as the detuning is increased with increasing $n_{\rm g}$. Moreover, ϕ has opposite signs in the ground $|\downarrow\rangle$ and excited $|\uparrow\rangle$ states of the CPB.

Qubit state transitions can be driven by applying an additional microwave of frequency ω_s , detuning $\Delta_{s,a} = \omega_s - \tilde{\omega}_a$, and power P_s to the input port of the resonator [see Fig. 1(a)]. On resonance ($\Delta_{s,a} = 0$) and for a continuous (cw) large amplitude spectroscopy drive, the qubit transition saturates and the populations in the excited and the ground states approach 1/2. In this case, the measured phase shift of the probe beam at ω_{rf} is expected to saturate at $\phi = 0$ [see Fig. 1(c)]. By sweeping the spectroscopy frequency ω_s and the gate charge n_g and *continuously* measuring ϕ , we have mapped out the energy level sepa-

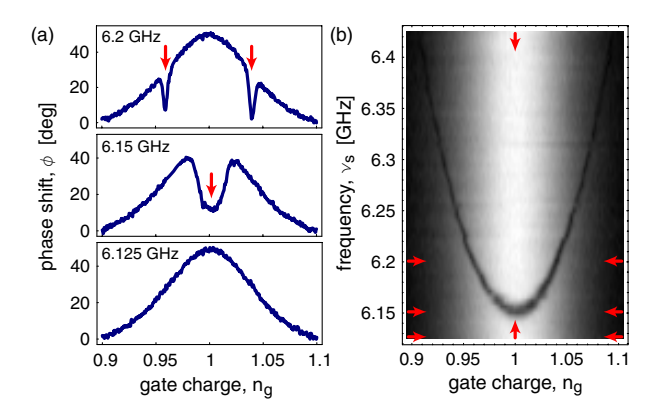


FIG. 2 (color online). (a) Probe microwave phase shift ϕ vs gate charge $n_{\rm g}$ at spectroscopy frequency $\nu_{\rm s}=6.125~{\rm GHz}$ (lower panel), 6.15 GHz (middle panel), and 6.2 GHz (upper panel). (b) Density plot of ϕ vs $n_{\rm g}$ and $\nu_{\rm s}$; white (black) corresponds to large (small) phase shift. Horizontal arrows indicate line cuts shown in (a); vertical arrows indicate line cuts shown in Fig. 4(a). Measurements in (a) and (b) were performed populating the resonator with $n\sim25$ photons on average.

ration $\tilde{\omega}_a$ of the qubit (see Fig. 2). In the lower panel of Fig. 2(a), the measured phase shift ϕ is shown for the nonresonant case, where $\omega_s < \tilde{\omega}_a$ for all values of gate charge n_g . The measured phase shift is, as expected, a continuous curve similar to the one shown in Fig. 1(c). In the middle panel of Fig. 2(a), the spectroscopy microwave at $\nu_s = \omega_s/2\pi = 6.15$ GHz is in resonance with the qubit at $n_g = 1$, populating the excited state and thus inducing a dip in the measured phase shift ϕ around $n_g = 1$, as expected. Note that, as predicted [4], our measurement scheme has the advantage of being most sensitive at charge degeneracy, a bias point where traditional electrometry, using a radio frequency single electron transistor [15], for example, is unable to distinguish the qubit states.

When ν_s is increased to higher values, resonance with the qubit occurs for two values of $n_{\rm g}$ situated symmetrically around $n_{\rm g}=1$, leading to two symmetric dips in ϕ [see upper panel of Fig. 2(a)]. From the $[n_g, \nu_s]$ positions of the spectroscopic lines in the measured phase ϕ , the Josephson energy $E_{\rm J} = 6.2$ GHz and the charging energy $E_{\rm C} = 4.8$ GHz are determined in a fit using the full qubit Hamiltonian beyond the two-level approximation [14] [see density plot of ϕ vs n_g and ν_s in Fig. 2(b)]. In this experiment the flux bias Φ_{b} has been chosen to result in a minimum detuning of about $\Delta_{\rm a,r}/2\pi\approx 100~{\rm MHz}$ at $n_{\rm g}=1$. The tunability of $E_{\rm J}$ (i.e., the detuning at charge degeneracy) has been demonstrated previously [5]. It is also worth noting that the spectroscopy frequency ω_s typically remains strongly detuned ($\Delta_{s,r} = \omega_s - \omega_r >$ $2\pi 100$ MHz) from the resonator, such that a large fraction of the spectroscopy photons are reflected at the input port and only a small number n_s , determined by the Lorentzian line shape of the resonator, populates the resonator.

Various other radio or microwave frequency qubit readout schemes have been developed recently [15–17]. In a related experiment, the level separation of a split Cooper pair box coupled *inductively* to a *low frequency, moderate* Q tank circuit has been determined spectroscopically [18].

The width and the saturation level of the spectroscopic lines discussed above depend sensitively on the power $P_{\rm s}$ of the spectroscopic drive. Both quantities are related to the excited state population

$$P_{\uparrow} = 1 - P_{\downarrow} = \frac{1}{2} \frac{n_s \omega_{\text{vac}}^2 T_1 T_2}{1 + (T_2 \Delta_{sa})^2 + n_s \omega_{\text{vac}}^2 T_1 T_2},$$
 (2)

found from the Bloch equations in steady state [19], where $\omega_{\rm vac} = 2g$ is the vacuum Rabi frequency, n_s the average number of spectroscopy photons in the resonator, T_1 the relaxation time, and T_2 the dephasing time of the qubit. We have extracted the transition linewidth and saturation from spectroscopy frequency scans for different drive powers P_s with the qubit biased at charge degeneracy ($n_g = 1$). We observe that the spectroscopic lines have a Lorentzian line shape with width and depth in accordance with Eq. (2). The

half width at half maximum (HWHM) of the line is found to follow the expected power dependence $2\pi\delta\nu_{\rm HWHM} =$ $1/T_2' = (1/T_2^2 + n_s \omega_{\text{vac}}^2 T_1/T_2)^{1/2}$ [19], where the input microwave power P_s is proportional to $n_s\omega_{\rm vac}^2$ [see Fig. 3(a)]. In the low power limit $(n_s\omega_{\rm vac}^2\to 0)$, the unbroadened linewidth is found to be small, $\delta \nu_{\rm HWHM} \approx$ 750 kHz, corresponding to a long dephasing time of T_2 200 ns at $n_g = 1$, where the qubit is only second order sensitive to charge fluctuations limiting the dephasing time in this sample. At a larger drive, the width increases proportionally to the drive amplitude. The depth of the spectroscopic dip at resonance ($\Delta_{s,a} = 0$) reflects the probability of the qubit to be in the excited state P_{\uparrow} and depends on P_s as predicted by Eq. (2) [see Fig. 3(b)]. At low drive the population increases linearly with P_s and then approaches 0.5 for large P_s . From time resolved measurements (data not shown), T_1 is found to be on the order of a few microseconds, a value which is much shorter than that expected for radiative decay of the qubit in the cavity [4], indicating the existence of other, possibly nonradiative decay channels.

In the above we have demonstrated that the strong coupling of the qubit to the radiation field modifies the resonator transition frequency in a way that can be exploited to measure the qubit state. Correspondingly, the resonator acts back onto the qubit through their mutual strong coupling. Regrouping the terms of the Hamiltonian in Eq. (1) one sees that the *dressed* qubit level separation is given by $\tilde{\omega}_a = \omega_a + 2 \text{ ng}^2/\Delta_{a,r} + g^2/\Delta_{a,r}$, where we note that the resonator gives rise to an ac Stark shift of the qubit levels of $\pm ng^2/\Delta_{a,r}$, proportional to the intraresonator photon number $n = \langle a^{\dagger} a \rangle$, as well as a Lamb shift $\pm g^2/2\Delta_{\rm a.r}$, due to the coupling to the vacuum fluctuations. The ac Stark shift is measured spectroscopically at $n_g = 1$ for fixed power P_s by varying the probe beam power P_{rf} which changes the average measurement photon number nin the resonator (see Fig. 4). We observe that the qubit level

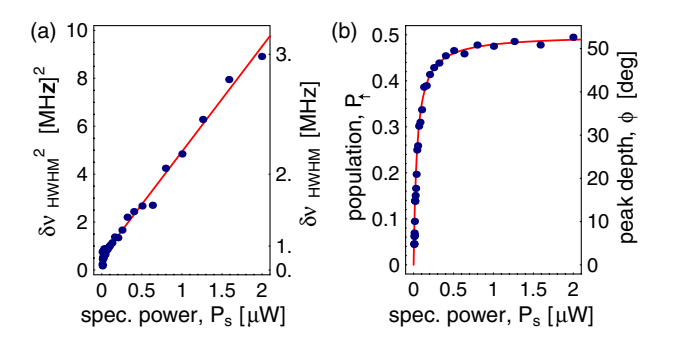


FIG. 3 (color online). (a) Measured qubit linewidth $\delta \nu_{\rm HWHM}$ vs input spectroscopy power P_s (solid circles) with fit (solid line). Probe beam power $P_{\rm rf}$ is adjusted such that n < 1. (b) Measured peak depth ϕ and excited state population probability P_{\uparrow} on resonance $\Delta_{\rm s,a} = 0$ vs $P_{\rm s}$ (solid circles) with fit (solid line).

separation $\tilde{\nu}_{\rm a} = \tilde{\omega}_{\rm a}/2\pi$ is linear in $P_{\rm rf}$ [see Fig. 5(a)], i.e., that the ac Stark shift $\nu_{\rm ac} = 2ng^2/2\pi\Delta_{\rm a,r}$ is linear in the photon number n, as expected. In the limit of $P_{\rm rf} \rightarrow 0$ ($n \rightarrow$ 0), the bare qubit level separation $\omega_a + g^2/\Delta_{a,r} = 2\pi$ 6.15 GHz is determined, where $g^2/\Delta_{a,r}$ is the small Lamb shift which cannot be separated from ω_a in our current experiments. Knowing the coupling constant g from an independent measurement of the vacuum Rabi mode splitting [5] and $\Delta_{a,r}$ from spectroscopic measurements in the $n \rightarrow 0$ limit, the dependence of the intraresonator photon number n on the input power P_{rf} is determined from the measured ac Stark shift $\nu_{\rm ac}$. We find that an input microwave power of $P_{\rm rf}=-29$ dBm corresponds to n = 1 which is consistent with an intended attenuation of approximately 105 dB in the input coaxial line. The ac Stark shift of the qubit at this particular detuning is a remarkable 0.6 MHz per photon in the cavity and is comparable to the linewidth. Using this method, the intraresonator photon number was calibrated to a precision of $\sim \pm 1$ dB for the vacuum Rabi mode splitting measurements presented in Ref. [5].

Quantum fluctuations (photon shot noise) δn around the average photon number n of the coherent field populating the resonator give rise to random fluctuations in the qubit transition frequency due to the ac Stark shift. This leads to measurement-induced dephasing, and thus to a broadening of the qubit linewidth (see Figs. 4 and 5). This is the measurement backaction and can be understood quantitatively by considering the relative phase $\varphi(t) = 2g^2/\Delta_{\rm a,r} \int_0^t dt' \delta n(t')$ accumulated in time between the ground and the excited states of the qubit. Following Ref. [4], the measurement-induced phase decay of the qubit is then characterized by

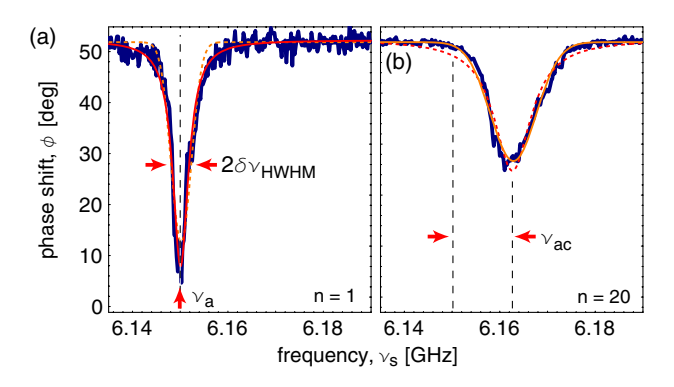


FIG. 4 (color online). Measured spectroscopic lines (wide lines with noise) at (a) intraresonator photon number $n\approx 1$ ($P_{\rm rf}=-30~{\rm dBm}$) with fit to Lorentzian line shape (solid line) and at (b) $n\approx 20~(P_{\rm rf}=-16~{\rm dBm})$ with fit to Gaussian line shape (solid line). Dashed lines are best fits to (a) Gaussian or (b) Lorentzian line shapes, respectively. The qubit transition frequency $\nu_{\rm a}$ at low $P_{\rm rf}$, the half width half maximum $\delta \nu_{\rm HWHM}$, and the ac Stark shift $\nu_{\rm ac}$ of the lines are indicated.

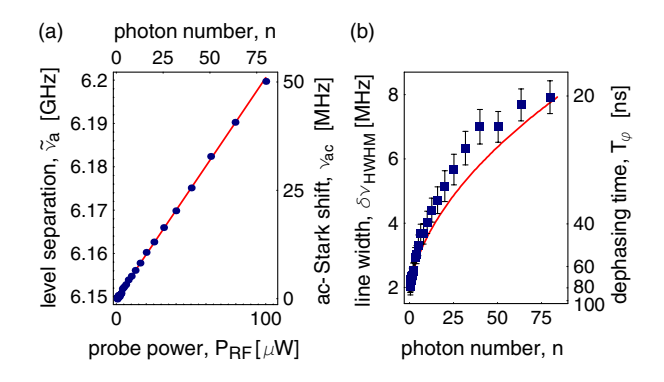


FIG. 5 (color online). (a) Measured qubit level separation $\tilde{\nu}_a$ and fit (solid line) vs input microwave probe power $P_{\rm rf}$. The ac Stark shift $\nu_{\rm ac}$ and the intraresonator photon number n extracted from the fit are also indicated. (b) Measurement broadened qubit linewidth $\delta \nu_{\rm HWHM}$ vs n. Error bars are reflecting estimated systematic uncertainties in the extracted linewidth. The corresponding total dephasing time $T_{\varphi} = 1/2\pi\delta\nu_{\rm HWHM}$ is also indicated. The solid line is obtained from Eq. (4) with a spectroscopy power broadened $T_2' \approx 80$ ns.

$$\langle e^{i\varphi(t)}\rangle = \exp\left[-\frac{2g^4}{\Delta_{\text{a.r}}^2} \iint_0^t dt_1 dt_2 \langle \delta n(t_1) \delta n(t_2) \rangle\right],$$
 (3)

where the fluctuations δn are assumed to be Gaussian. In the above expression, the photon correlation function $\langle \delta n(t) \delta n(0) \rangle = n \exp(-\kappa |t|/2)$ of the coherent probe beam in the resonator is governed by the cavity decay rate κ and physically represents the white photon shot noise filtered by the cavity response. The spectroscopic line shape $S(\omega)$ is obtained from the Fourier transform of $\langle \exp[i\varphi(t)] \rangle e^{-t/T_2'}$, where $1/T_2'$ takes into account dephasing mechanisms independent of the measurement

$$S(\omega) = \frac{1}{\pi} \sum_{j=0}^{\infty} \frac{(-4\chi)^j}{j!} \frac{1/T_2' + 2\kappa\chi + j\kappa/2}{(\omega - \tilde{\omega}_a)^2 + (\frac{1}{T_2'} + 2\kappa\chi + \frac{j\kappa}{2})^2}.$$
(4)

The form of the line shape depends on the dimensionless parameter $\chi = n\theta_0^2$, where $\theta_0 = 2g^2/\kappa \Delta_{\rm a,r}$ is the transmission phase shift describing the strength of the measurement. For small χ the measurement rate is slow compared to κ and the phase diffuses in a random walk $\langle \varphi(t)^2 \rangle \sim$ $4\theta_0^2 n \kappa t$, leading to a homogeneously broadened Lorentzian line of HWHM of $2\theta_0^2 n\kappa + 1/T_2'$. For large χ , i.e., strong measurement, the measurement rate exceeds κ leading to a qubit transition frequency which depends on the instantaneous value of the cavity photon number and hence to an inhomogeneously broadened Gaussian line [see Fig. 4(b)], whose variance is simply \sqrt{n} multiplied by the Stark shift per photon. The full crossover from intrinsic Lorentzian line shape with width $\propto n$ at small n to Gaussian line shape with width $\propto \sqrt{n}$ at large n as described by Eq. (4) with no adjustable parameters is in good agreement with the measured dependence of the linewidth on n [see Fig. 5(b)]. The slightly increased measured linewidth could be attributed to fluctuations (e.g., charge noise) activated at high photon numbers and to the nonlinearity of the ac Stark shift above the critical photon number [4]. We note that this effect is not seen in Fig. 4(a) because of compensation by the change of the cavity pull at large n from the zero-photon limit g^2/Δ .

In our experiments we have demonstrated that the strong coupling of a Cooper pair box to a nonresonant microwave field in an on-chip cavity gives rise to a large qubit dependent shift in the excitation energy of the resonator. The ac Stark effect shifts the qubit level separation by about one linewidth per photon at 2% detuning, and the backaction of the fluctuations in the field gives rise to a large broadening of the qubit line. Good agreement of the line shape with theory indicates that the dispersive measurement is QND, as expected.

We thank M. Devoret and I. Chiorescu for discussions. This work was supported in part by NSA and ARDA under ARO Contract No. DAAD19-02-1-0045, and the NSF under Grants No. ITR-0325580 and No. DMR-0342157, the David and Lucile Packard Foundation, the W. M. Keck Foundation, and the NSERC of Canada.

- *Also at Ames Laboratory, Iowa State University, Ames, IA 50011, USA.
- [1] H. Mabuchi and A. Doherty, Science 298, 1372 (2002).
- [2] D. Walls and G. Milburn, *Quantum Optics* (Spinger-Verlag, Berlin, 1994).
- [3] M. A. Nielsen and I. L. Chuang, *Quantum Computation* and *Quantum Information* (Cambridge University Press, Cambridge, U.K., 2000).
- [4] A. Blais et al., Phys. Rev. A 69, 062320 (2004).
- [5] A. Wallraff et al., Nature (London) 431, 162 (2004).
- [6] I. Chiorescu et al., Nature (London) 431, 159 (2004).
- [7] Y. Nakamura, Y.A. Pashkin, and J.S. Tsai, Nature (London) 398, 786 (1999); D. Vion et al., Science 296, 886 (2002); J.M. Martinis, S. Nam, J. Aumentado, and C. Urbina, Phys. Rev. Lett. 89, 117901 (2002); Y. Yu et al., Science 296, 889 (2002); I. Chiorescu, Y. Nakmura, C.J.P.M. Harmans, and J.E. Mooij, Science 299, 1869 (2003); T. Yamamoto et al., Nature (London) 425, 941 (2003).
- [8] T. Yoshie et al., Nature (London) 432, 200 (2004).
- [9] J. P. Reithmaier *et al.*, Nature (London) **432**, 197 (2004).
- [10] V. Bouchiat et al., Phys. Scr. **T76**, 165 (1998).
- [11] P. Grangier, J.A. Levenson, and J.-P. Poziat, Nature (London) 396, 537 (1998).
- [12] G. Nogues et al., Nature (London) 400, 239 (1999).
- [13] P. Brune et al., Phys. Rev. Lett. 72, 3339 (1994).
- [14] Y. Makhlin, G. Schön, and A. Shnirman, Rev. Mod. Phys. 73, 357 (2001).
- [15] K. Lehnert et al., Phys. Rev. Lett. 90, 027002 (2003).
- [16] A. Lupascu et al., Phys. Rev. Lett. 93, 177006 (2004).
- [17] I. Siddiqi et al., Phys. Rev. Lett. 93, 207002 (2004).
- [18] D. Born et al., Phys. Rev. B 70, 180501 (2004).
- [19] A. Abragam, The Principles of Nuclear Magnetism (Oxford University Press, Oxford, 1961).